J. Fluid Mech. (1995), *vol.* 304, *pp.* 161–183

Longitudinal streaks

By MARCO COLOMBINI[1] AND GARY PARKER[2]

[1]Istituto Idraulica, Università degli Studi di Genova, 16145 Genova, Italy

[2]St. Anthony Falls Hydraulics Laboratory, University of Minnesota, Minneapolis, MN 55414, USA

(Received 14 October 1994 and in revised form 10 May 1995)

A commonly observed bedform in wide erodible-bed channels consists of rows of streaks or stripes parallel to the flow. These stripes can be manifested in terms of transverse variation of bed elevation, characteristic grain size (and thus roughness) or both. The former case is manifested most strongly in sediment with a nearly uniform size distribution and the latter most strongly in sediment with substantial heterogeneity in size. The amplitude of stripes is rarely larger than one or two grain diameters, and the transverse spacing is invariably of the order of the flow depth. They are closely linked to a pattern of paired cells of secondary flow in the flow cross-section.

An existing theory of streak formation for the case of uniform sediment relies on a second-order turbulence closure which explicitly links the streamwise flow to transverse variations in bed elevation. The theory successfully predicts the formation of streaks, but only at rather high values of the Shields stress, i.e. rather strong sediment transport. Streaks are commonly observed, however, at Shields stresses as low as only slightly above the threshold of motion.

In the present analysis the previous flow model is adapted to the case of transverse variation of roughness as well as elevation, and the constraint of uniform sediment is removed. The theory indicates that allowance for even slight heterogeneity of bed sediment results in the formation of streaks at any Shields stress above the threshold of motion. The resulting streaks are hybrid in the sense that they show transverse variation in both elevation and roughness. The model thus provides a general theory of streak formation.

1. Introduction

The formation of longitudinal stripes of sediment in wide straight channels can be observed in laboratory experiments over a wide range of flow and sediment parameters. They appear to be more evident in the initial stage of motion, before more prominent bedforms such as ripples, dunes or bars become manifest. Longitudinal streaks, characterized usually by a very small amplitude (one or two grain diameters), appear as perturbations in bed elevation if the sediment is homogeneous and as stripes of different roughness if the sediment is heterogeneous. They tend to be remarkably uniform in the streamwise direction and periodic in the spanwise direction with a periodicity that is invariably of the order of the flow depth. That is, typical wavelengths vary from one to two times the flow depth. For example, Wolman & Brush (1961), Kinoshita (1967), Ashida & Narai (1969) and Ikeda (1981) find spacing near twice the flow depth. These references encompass a data base that includes both laboratory channels and rivers.

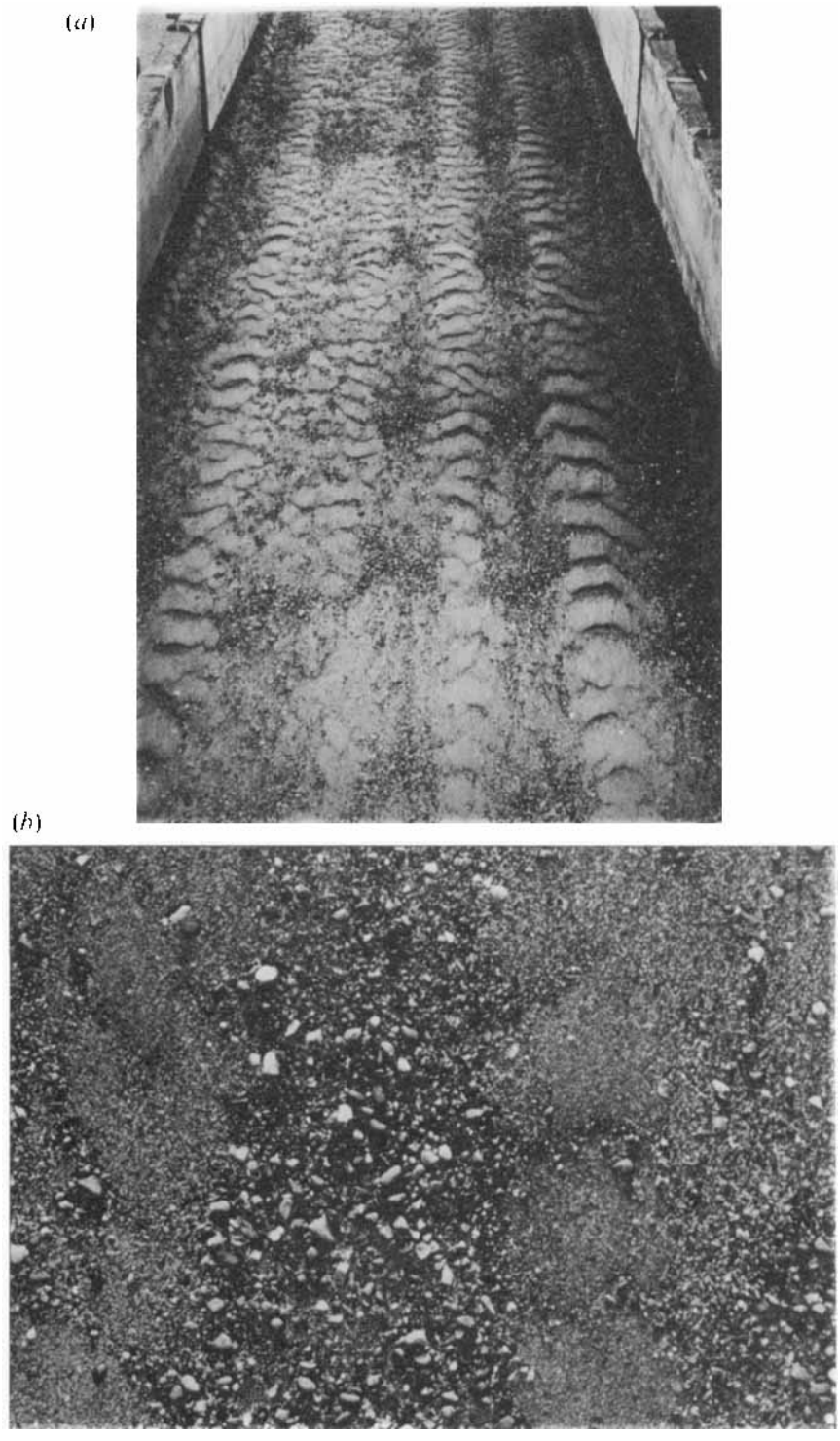

FIGURE 1. Longitudinal streaks, Günter (1971): (*a*) the characteristic pattern of alternating stripes; (*b*) a close up of the bed showing the effect of sorting. Flow is from bottom to top.

Streaks (see figure 1) are associated with the presence of secondary flow in the cross-section. It has been demonstrated both numerically and experimentally that lateral variations either in the bed roughness or in the bed elevation are able to induce secondary motions that, in turn, can excite the amplification of these bed perturbations eventually leading to a stable configuration (Müller & Studerus 1979; Nezu & Nakagawa 1984; Tsujimoto 1989). Most experimental work has, then, been devoted to the study of the structure and intensity of the secondary flow generated by the two mechanisms, in attempts to shed some light on the phenomenon. The two mechanisms are, however, clearly interrelated when the sediment is heterogeneous, as is the case in nature. It can be easily demonstrated that the process of sorting on the bed that leads to the formation of lateral roughness stripes is also responsible for lateral changes in bed elevation so that, at least theoretically, the two mechanisms are not separable.

As in many other studies on bedform formation, linear stability analysis is a powerful tool to extract useful information about the occurrence of streaks and on their most important geometric characteristics. The well-established quasi-steady assumption exploits the considerable difference between the characteristic timescales of flow and bed evolution to allow for temporal decoupling of the system of flow equations from the continuity equations for each sediment fraction. The response of a uniform flow field to a 'fixed' bed perturbation either in roughness or in elevation, and the time evolution of these disturbances can then be analysed separately.

The first step in this direction is the elaboration of the simplest possible flow model able to correctly predict the effect of lateral bed variation either in roughness or in elevation. A comparison with experiments over a fixed bed will then be possible for both cases.

The formulation of such a model, however, is not a trivial task, owing to the rather arcane mechanism by which secondary flow is generated in the cross-section of a straight channel. Since the first analysis carried out by Prandtl (see Bradshaw 1987) it has been recognized that straight-channel secondary flow can be modelled only using a turbulence closure able to provide an accurate description of the variation of Reynolds stresses in the cross-sectional plane. All turbulence closures that assume a linear dependence of the Reynolds stress tensor on the mean rate of strain tensor (i.e. the so-called Boussinesq closures) are known to fail for this configuration. Attention must then be focused on more refined second-order turbulence models. Unfortunately these models are often formulated in an implicit way and are not suitable for the analytic solution that would be desirable in the present context, where the assumption of infinitesimal disturbances strongly simplifies the analysis.

In a previous work (Colombini 1993), one of the authors successfully adopted the model of Speziale (1987) to study the formation of sand ridges, i.e. the longitudinal bedforms associated with uniform sediment. The same model is adopted here with the inclusion of the effect of lateral variation of bed roughness in order to perform a complete stability analysis of the formation of streaks formed in heterogeneous sediment. This generalization immediately leads to an interesting thought problem.

Let us formulate the problem for the two limiting cases sketched in figure 2: (*a*) flow over a uniform bed with a sinusoidal lateral variation in bed elevation and (*b*) flow over a flat bed with a sinusoidal lateral variation in the bed roughness.

The effect of changes in bed roughness on the flow field may be interpreted in terms of variation in the 'reference level', i.e. the distance from the bed at which the mean velocity is assumed to be zero. This distance is proportional to the local value of the bed roughness.

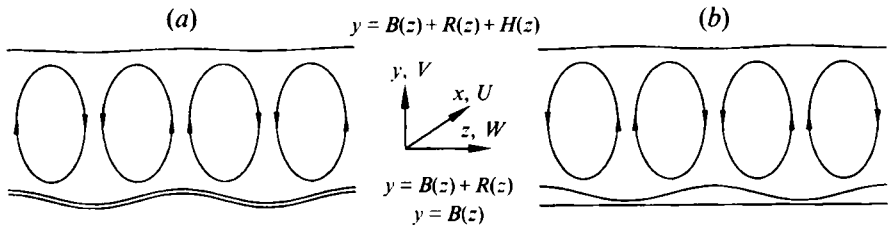

FIGURE 2. Sketches of flow configuration: (*a*) perturbation of the bed elevation with a uniform sediment; (*b*) perturbation of the bed roughness with a flat bed. Here B, H and R are the local values of bed elevation, flow depth, and the distance between the reference level and the bed.

At first glance the flow domains in the two cases appear to be identical. It is found in case (*a*) that the transverse flow in the near-bed region moves from trough to crest. This in turn drives the instability by which the streaks grow in amplitude over a uniform bed (Colombini 1993). A naive generalisation of the results of case (*a*) to case (*b*) would suggest that the transverse secondary flow be directed from low reference level (fine sediment) to high reference level (coarse sediment). This conclusion is in complete disagreement with observation (McLean 1981; Tominaga & Nezu 1991). It also implies that straight-channel secondary currents stabilize roughness streaks rather than drive them. That is, the same mechanism that causes elevation streaks over uniform sediment obliterates roughness streaks over heterogeneous sediment. In the section devoted to the flow field solution the naive generalization leading to this conclusion will be shown to be incorrect. It will be shown that both elevation and roughness streaks can be explained using the same model for straight-channel secondary currents.

It is convenient at this point to briefly summarize some of the salient concepts and results of the theory of formation of sand ridges with homogeneous sediment. For a more complete analysis the reader may refer to Colombini (1993).

The use of the Speziale turbulence closure allows for the formulation of a model for the flow field over a sinusoidal bottom of infinitesimal amplitude as a small perturbation of the uniform flow in an infinitely wide open channel. A comparison with the experimental results of Nezu & Nakagawa (1984) was performed in order to obtain optimal values for the two constants C_D and C_E involved in Speziale's formulation. It was found that values higher than those originally proposed by Speziale had to be used in order to obtain a correct description of the Reynolds stresses in the cross-sectional plane and consequently a predicted secondary flow of the correct intensity. A value of 3.4 for both constants, as opposed to the original value of 1.69, provided optimal agreement.

The sign of the growth rate, and so the amplification or decay of the bed perturbations, was shown to be controlled by a delicate balance between a destabilizing term related to the tangential shear stress at the bed, and a stabilizing term related to the effect of gravity. The tangential shear stress at the bottom was found to be underestimated by the theory, with a corresponding overestimation of the critical value for the occurrence of sand ridges. Sand ridges were predicted to appear only at relatively large values of the Froude number, whereas experimental observations show that sand ridges occur also at lower values of the Froude number, limited only by the threshold for grain motion. The estimate of characteristic transverse wavelength, or streaks spacing, was obtained using the standard technique of linear stability theory, i.e. by maximizing the growth rate. The prediction for an infinitely wide channel

agreed reasonably well with the result of experiments in channel wide enough to allow for the neglect of sidewall effects. The predicted values for wavelength were near 1.3 times the flow depth for a wide range of flow and sediment parameters. This number compares with measured wavelength between 1 and 2 times the depth, with the upper limit more common, as quoted above.

Regarding the stability criterion it must be pointed out that its formulation in terms of the Froude number, as originally presented in the paper, is formally correct but nevertheless misleading. The role played in the analysis by the Froude number is indeed a very minor one, related to the small effect of the undulations of the free surface. The dominant flow parameter mechanistically associated with instability is the Shields stress; it is incidental that this parameter can be recast in terms of the Froude number. Instability is found for values of the Shields stress of order 1.

As will be shown later, the theory for a heterogeneous sediment presented here predicts instability for all values of the Shields stress above the threshold for motion. This provides a general explanation of the occurrence of sand ridges at low Shields stresses in nature, where the sediment can normally be expected to show significant heterogeneity.

2. Turbulence closure

As mentioned in the introduction, a correct prediction of the behaviour of the Reynolds stresses in the cross-sectional plane is of fundamental importance in the modelling of secondary flow. In order to illustrate this, consider the equation of streamwise vorticity for a turbulent flow that is uniform in the streamwise direction. Neglecting the viscous term, it takes the form

$$\frac{\partial \omega}{\partial t} + V\frac{\partial \omega}{\partial y} + W\frac{\partial \omega}{\partial z} = \frac{\partial^2}{\partial y \partial z}(\tau_{zz} - \tau_{yy}) + \left(\frac{\partial^2}{\partial y^2} - \frac{\partial^2}{\partial z^2}\right)\tau_{yz}, \tag{2.1a}$$

with

$$\omega = \frac{\partial V}{\partial z} - \frac{\partial W}{\partial y}. \tag{2.1b}$$

If a closure of Boussinesq type is employed, all the terms of the previous equation are found to depend on the secondary flow velocities V and W only, so that the equation is completely decoupled from the streamwise momentum equation. A uniform unidirectional flow, with no secondary flow, may then prevail in the presence of an arbitrary lateral perturbation of the bed shape (or of the profile of the reference level) since the trivial solution $V = 0$ and $W = 0$ always satisfies equation (2.1*a*). The analogy with the laminar case, where no secondary flow can be generated by varying boundary shape, can be illuminating. In this case the streamwise vorticity equation reads

$$\frac{\partial \omega}{\partial t} + V\frac{\partial \omega}{\partial y} + W\frac{\partial \omega}{\partial z} = \nu\left(\frac{\partial^2}{\partial y^2} + \frac{\partial^2}{\partial z^2}\right)\omega. \tag{2.2}$$

The equation is again identically satisfied if V and W are zero.

This inconsistency can be overcome by choosing a second-order turbulence closure to model the Reynolds stresses, as this enforces a coupling between the streamwise vorticity and momentum equations. Several choices are available; in fact the problem of secondary flow in a square duct has been successfully solved using algebraic stress models (Naot & Rodi 1982; Demuren & Rodi 1984), and can in principle be obtained from a more general solution involving transport equations for each individual stress.

As in Colombini (1993) the turbulence model of Speziale (1987) has been adopted here by virtue of its structure, which allows for some drastic simplifications without losing the ability to provide a good description of the secondary flow.

Speziale's model is in fact an explicit model, with a simple structure that requires only two new non-dimensional constants, an eddy viscosity and a mixing length, in order to achieve closure. This is particularly suitable here because slight perturbations of a uniform unidirectional flow are considered. This suggests the utility of modelling the eddy viscosity and the mixing length using algebraic relationships known to hold for a uniform flow.

In a recent paper Gatski & Speziale (1993) have formally demonstrated that second-order closures can be seen as explicit generalized forms of algebraic stress models. It is then not unexpected that a close similarity exists between the linearized form of the Reynolds stresses obtained using Speziale's model and an algebraic stress closure (Naot & Rodi 1982).

Speziale assumed a functional dependence of the Reynolds stress tensor of the kind

$$\tau = \tau\left[\nabla\bar{v}, \frac{\mathrm{D}(\nabla\bar{v})}{\mathrm{D}t}, \rho, k, l\right], \tag{2.3}$$

where $\bar{v}$ is the velocity vector and ρ, k, l are the fluid density, the turbulent kinetic energy and the turbulence lengthscale respectively.

Imposing some general constraints on this functional, in particular coordinate and dimensional invariance, positiveness of the turbulent kinetic energy and frame-indifference, Speziale derived at second-order the following explicit form for the Reynolds stresses:

$$\tau_{ij} = -\tfrac{2}{3}k\delta_{ij} + 2\nu_t D_{ij} + C_D l^2(D_{im}D_{mj} - \tfrac{1}{3}D_{mn}D_{mn}\delta_{ij}) + C_E l^2(\widehat{D}_{ij} - \tfrac{1}{3}\widehat{D}_{mm}\delta_{ij}). \tag{2.4a}$$

Here D_{ij} is the mean rate of strain tensor, $\nu_t = \frac{1}{2}k^{1/2}l$ is the eddy viscosity and

$$\widehat{D}_{ij} = \frac{\mathrm{D}D_{ij}}{\mathrm{D}t} - \frac{\partial U_i}{\partial x_k}D_{kj} - \frac{\partial U_j}{\partial x_k}D_{ki} \tag{2.4b}$$

is the Oldroyd derivative of D_{ij}.

In the paper by Gatski & Speziale (1993) the same constitutive relationship, with the convective term in the Oldroyd derivative dropped, is obtained as a particular case of a more general family of higher-order explicit turbulence closures. The inclusion of a more refined turbulent closure, even though likely to improve the agreement with the experiments (see the discussion in Colombini 1993), is likely beyond the scope of the present contribution; with this in mind the original formulation of Speziale (1987) is used here as well.

The eddy viscosity and the turbulence lengthscale are modelled using the mixing length hypothesis as described in De Vriend (1977), with the mixing length l chosen so as to produce a logarithmic vertical profile of velocity for the base flow. Thus

$$\nu_t = l^2\frac{\partial U}{\partial y}, \qquad l = \kappa(y - B)\left(\frac{B + R + H - y}{H}\right)^{1/2}, \tag{2.5a,b}$$

where κ is the von Kármán constant, taken as 0.4, and B, H and R are the local values of bed elevation, flow depth, and the distance between the reference level and the bed, respectively, as shown in figure 2.

That (2.5) does indeed result in the standard rough logarithmic profile for the base flow can be seen as follows. In the absence of secondary flow, the streamwise

momentum balance for a steady equilibrium base flow reduces to

$$\tau_{xy} = \rho u_*^2 \frac{B + R + H - y}{H}, \tag{2.6}$$

where u_* is the friction velocity of the base flow. Note that $y = B + R + H$ denotes the elevation of the water surface and $y = B + R$ denotes the reference level, at which the base streamwise velocity U_0 vanishes, i.e.

$$U_0|_{y=B+R} = 0. \tag{2.7}$$

Completing (2.5) and (2.6) with the closure hypothesis

$$\tau_{xy} = \rho \left(l \frac{\partial U_0}{\partial y} \right)^2, \tag{2.8}$$

and integrating subject to (2.7), it is found that

$$\frac{U_0}{u_*} = \frac{1}{\kappa} \ln \left(\frac{y - B}{R} \right), \tag{2.9}$$

i.e. the rough logarithmic law.

Note that B and R are not symmetric in relation (2.5) for mixing length l. This asymmetry is responsible for a pattern of secondary flow near the bed that is directed from low B to high B in the case of constant R, but from high R to low R in the case of constant B, as outlined below.

3. Linearized flow field solution

In this section the flow field resulting from the perturbation of a uniform flow due to spanwise-periodic disturbances of the bed shape and roughness is studied. All the quantities that appear in this section have been made dimensionless using the fluid density ρ, the friction velocity u_* and the flow depth of the basic uniform flow.

The bed topography usually evolves on a much slower timescale than that of the flow field, making it possible to neglect all the time derivatives in the three-dimensional Reynolds equations, or, equivalently, to assume that the flow adapts itself instantaneously to changes in bed elevation and structure. The momentum and continuity equations can then be written in the following form:

$$V \frac{\partial U}{\partial y} + W \frac{\partial U}{\partial z} = 1 + \frac{\partial \tau_{xy}}{\partial y} + \frac{\partial \tau_{xz}}{\partial z}, \tag{3.1a}$$

$$V \frac{\partial V}{\partial y} + W \frac{\partial V}{\partial z} = -\frac{\partial P}{\partial y} + \frac{\partial \tau_{yy}}{\partial y} + \frac{\partial \tau_{yz}}{\partial z}, \tag{3.1b}$$

$$V \frac{\partial W}{\partial y} + W \frac{\partial W}{\partial z} = -\frac{\partial P}{\partial z} + \frac{\partial \tau_{yz}}{\partial y} + \frac{\partial \tau_{zz}}{\partial z}, \tag{3.1c}$$

$$\frac{\partial V}{\partial y} + \frac{\partial W}{\partial z} = 0, \tag{3.1d}$$

where P is the dynamic pressure. The uniform flow to be perturbed is chosen so as to satisfy the equations of motion.

The following decomposition is introduced into the differential system (3.1) to investigate the behaviour of a disturbance with growth rate Ω (defined on an appropriately slow timescale in order to follow the evolution of the sediment processes) and

wavenumber α:

$$(U, V, P) = (U_0(y), 0, P_0(y)) + \epsilon(u(y), v(y), p(y))E(t)C(z), \tag{3.2a}$$

$$W = -\epsilon\alpha w(y)E(t)S(z), \tag{3.2b}$$

$$(B, H, R) = (0, 1, R_0) + \epsilon(b, h, r)E(t)C(z), \tag{3.2c}$$

$$(\nu_t, l) = (\nu_{t0}(y), l_0(y)) + \epsilon(\nu_{t1}(y), l_1(y))E(t)C(z), \tag{3.2d}$$

$$k_s = k_{s0} + \epsilon k_{s1}E(t)C(z). \tag{3.2e}$$

Here ϵ is a small (strictly infinitesimal) parameter and

$$E(t) = \exp(\Omega t), \qquad C(z) = \cos(\alpha z), \qquad S(z) = \sin(\alpha z).$$

The non-orthogonal coordinate transformation

$$\eta = \frac{y - B(z) - R(z)}{H(z)}, \qquad \zeta = z, \tag{3.3a,b}$$

which maps the cross-section on a rectangular domain, is now introduced. Using the above transformation the free surface is identified by $\eta = 1$, while $\eta = 0$ identifies the reference level $y = B(z) + R(z)$.

The distance above the bed where the boundary condition of zero velocity is applied is chosen to be proportional to the local roughness height, so that

$$R = \frac{k_s}{30} \tag{3.4}$$

where k_s is the local value of relative roughness, again proportional to a suitable measure of the grain size.

Making the necessary substitutions and collecting terms at leading order, the system of differential equations for the basic uniform flow becomes

$$\nu'_{t0}U'_0 + \nu_{t0}U''_0 = -1, \tag{3.5a}$$

$$P'_0 = \tfrac{1}{12}C_D + \tfrac{1}{3}C_E \tag{3.5b}$$

where the primes denote derivatives with respect to η.

The above system is solved with the boundary conditions of vanishing velocity at $\eta = 0$ and of vanishing shear stress at the free surface, recovering the usual logarithmic distribution for the longitudinal velocity.

The mixing length and eddy viscosity for the basic flow are found to take the forms

$$l_0 = \kappa(R_0 + \eta)(1 - \eta)^{1/2}, \qquad \nu_{t0} = l_0^2 U'_0 = \kappa(R_0 + \eta)(1 - \eta), \tag{3.6a,b}$$

where

$$R_0 = \frac{k_{s0}}{30}. \tag{3.6c}$$

Owing to the smallness of R_0, typical values of which are of the order of one tenth of the non-dimensional grain size, we have neglected R_0 with respect to 1 in the above and in the following equations.

At first order in ϵ, perturbations of (2.5) lead to the following relationships:

$$l_1 = l_0 A, \qquad \nu_{t1} = \nu_{t0}\left(\frac{u'}{U'_0} + 2A - h\right), \tag{3.7a,b}$$

where

$$A = \frac{R_0 r + \eta h}{R_0 + \eta}, \qquad r = \frac{k_{s1}}{k_{s0}}. \tag{3.7c,d}$$

Here r is a normalized amplitude of the perturbation of the roughness height, which is given more precisely by ϵr.

It is now possible to address the conundrum presented in the Introduction and figure 2. The values $b = 1$ and $r = 0$ corresponds to case (a), and the values $b = 0$ and $r = 1$ corresponds to case (b). Assuming for simplicity that the free surface is flat, it is seen that

$$H = 1 - B - R, \qquad h = -b - R_0 r. \tag{3.8a,b}$$

The transformation (3.3) now reads

$$\eta = \frac{y - B - R}{1 - B - R}, \qquad \zeta = z, \tag{3.9a,b}$$

from which it is evident that B and R play identical roles. The function A, on the other hand, differs between the two cases:

$$A_{(a)} = \frac{-b\eta}{R_0 + \eta}, \qquad A_{(b)} = \frac{R_0 r(1 - \eta)}{R_0 + \eta}. \tag{3.10a,b}$$

The function A is seen to be proportional to $-\eta$ for case (a) and to $(1 - \eta)$ for case (b). This effect is therefore responsible for the different rotation of the secondary flow in the two cases.

Collecting the terms of order ϵ in (3.1) and substituting (3.5), (3.6) and (3.7), a system of ordinary differential equations of the following general form is eventually obtained:

$$\mathbf{D}\boldsymbol{Z} = h\boldsymbol{H} + b\boldsymbol{B} + r\boldsymbol{R}. \tag{3.11}$$

Here h is considered as a parameter to be determined and

$$\boldsymbol{Z} = \begin{pmatrix} u \\ v \\ w \\ p \end{pmatrix}.$$

The linear differential operator $\mathbf{D}$ is the same as the one reported in Appendix A of Colombini (1993). The three vectors $\boldsymbol{H}, \boldsymbol{B}$ and $\boldsymbol{R}$, which depend only on basic flow quantities, are

$$\boldsymbol{H} = \begin{pmatrix} -3 + \dfrac{2\eta}{R_0 + \eta} - (1 - \eta)\left(\dfrac{2R_0}{(R_0 + \eta)^2} + \alpha^2\eta\right) \\ -\left(\frac{1}{12}C_D + \frac{1}{3}C_E\right)\left(2 - \dfrac{2\eta}{R_0 + \eta}\right) - (1 - \eta)\left[\left(\frac{1}{12}C_D + \frac{1}{3}C_E\right)\dfrac{2R_0}{(R_0 + \eta)^2} + \frac{1}{4}C_D\alpha^2\eta\right] \\ -(1 - \eta)\left[\left(\frac{1}{12}C_D - \frac{2}{3}C_E\right) + \left(-\frac{1}{6}C_D + \frac{1}{3}C_E\right)\dfrac{2\eta}{R_0 + \eta}\right] \\ 0 \end{pmatrix},$$

$$\boldsymbol{B} = \begin{pmatrix} -\alpha^2(1 - \eta) \\ -\frac{1}{4}C_D\alpha^2(1 - \eta) \\ 0 \\ 0 \end{pmatrix},$$

$$\boldsymbol{R} = \begin{pmatrix} \dfrac{2R_0}{R_0+\eta} - (1-\eta)\left(-\dfrac{2R_0}{(R_0+\eta)^2} + \alpha^2 R_0\right) \\ \left(\frac{1}{12}C_D + \frac{1}{3}C_E\right)\dfrac{2R_0}{R_0+\eta} + (1-\eta)\left[\left(\frac{1}{12}C_D + \frac{1}{3}C_E\right)\dfrac{2R_0}{(R_0+\eta)^2} - \frac{1}{4}C_D\alpha^2 R_0\right] \\ -(1-\eta)\left(-\frac{1}{6}C_D + \frac{1}{3}C_E\right)\dfrac{2R_0}{R_0+\eta} \\ 0 \end{pmatrix}.$$

The above system must be solved so as to satisfy the boundary conditions of vanishing velocities at the lower boundary and the dynamic and kinematic boundary conditions at the free surface. The solution has been obtained numerically using a shooting method with a Runge–Kutta integration scheme.

More precisely, linearity of the differential system allows us to express its solution in the form

$$\boldsymbol{Z} = \sum_{i=1}^{3} c_i \boldsymbol{Z}_i + h\boldsymbol{Z}_h + b\boldsymbol{Z}_b + r\boldsymbol{Z}_r. \tag{3.12}$$

Thus $\boldsymbol{Z}$ is a linear combination of three linearly independent solutions of the homogeneous initial value problem

$$\mathbf{D}\boldsymbol{Z} = 0$$

each satisfying the boundary conditions at the lower boundary, plus particular solutions of the non-homogeneous differential systems

$$\mathbf{D}\boldsymbol{Z} = \boldsymbol{H}, \qquad \mathbf{D}\boldsymbol{Z} = \boldsymbol{B}, \qquad \mathbf{D}\boldsymbol{Z} = \boldsymbol{R}$$

also satisfying the lower boundary conditions.

The constants c_1, c_2, c_3 and h are then determined by solving the linear algebraic non-homogeneous systems obtained by imposing the remaining conditions at the upper boundary.

Once the system has been solved, the secondary flow is known for every value of the parameters up to the values of b and r. One quantity that is crucial in a description of the secondary flow and its effect on the bed evolution is the tangential component of the shear stress at the bottom. Following the above definitions, it is found that

$$\tau_t = -\epsilon\alpha(t_b b + t_r r)E(t)S(z) \tag{3.13a}$$

$$t_b = [v_{t0}w']^b, \qquad t_r = [v_{t0}w']^r \tag{3.13b,c}$$

where t_b and t_r are evaluated at the reference level and the limits b and r identify cases (a) and (b) respectively.

In figure 3 the quantities t_b and t_r are plotted as functions of the wavenumber α with the relative roughness k_{s0} as a parameter. As mentioned in the introduction, these quantities also have a formal direct dependence on the Froude number, but the dependence is so weak that no change is detectable in the plots as the Froude number is varied over the relevant range (0.1–2.0). According to (3.13) a positive value of t_b or t_r corresponds to a tangential bed shear stress that is negative in the first and second quadrants and positive in the remaining two. The opposite is true for a negative value. Therefore the near-bed flow is directed from trough to crest in case (a) and from the rough part to the smooth part in case (b) in accordance with

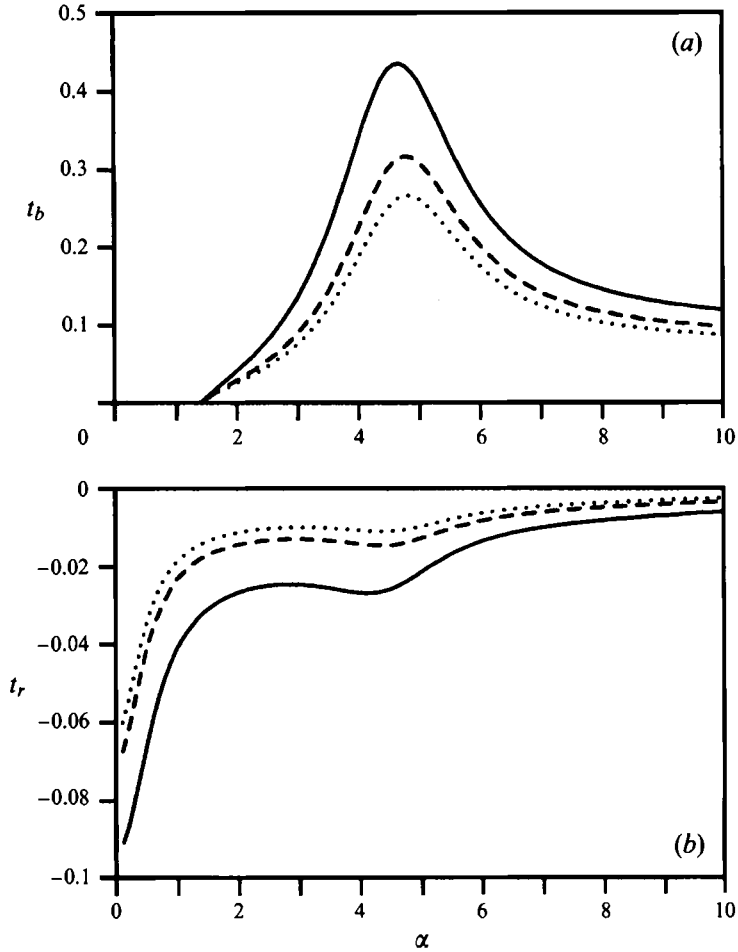

FIGURE 3. (*a*) t_b and (*b*) t_r as a function of the wavenumber α for different values of the relative roughness k_{s0}: ——, $k_{s0} = 0.125$; – – – –, $k_{s0} = 0.025$; · · · · · ·, $k_{s0} = 0.0125$.

the experimental observations. The apparent contradiction between the two has thus been resolved.

4. Bedload transport of sediment mixtures

Further progress on the subject of roughness streaks requires a formulation for the bedload transport of heterogeneous sediment. There are several such formulations in the literature; here the treatments of Parker & Sutherland (1990) and Parker (1990*a*,*b*) are used. The scheme of non-dimensionalization employed in the previous section is not used in this section.

Grain size D, which may be ascribed a specific value for homogeneous sediment, becomes a continuously distributed variable for heterogeneous sediment. The associated distribution of sizes is appropriately formulated in terms of the logarithm of D rather than D itself. The customary logarithmic scale of sedimentology is the phi scale, according to which

$$D = 2^{-\Phi}. \tag{4.1}$$

This scale is, however, counterintuitive in that increasing Φ corresponds to de-

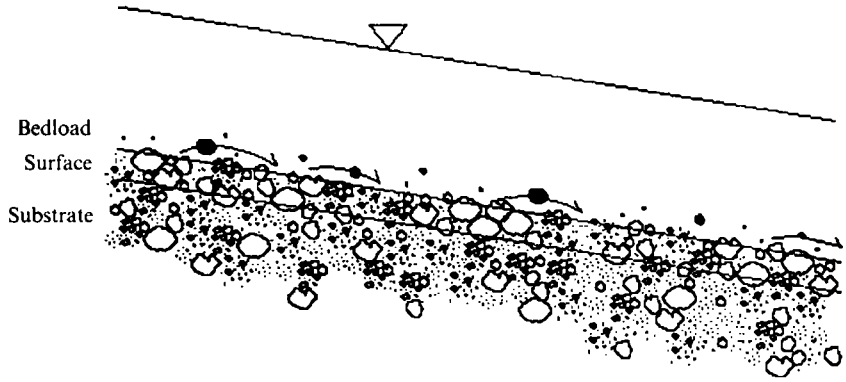

FIGURE 4. Sketch of the three-layer model for sediment transport

creasing grain size. With this in mind the psi scale (Parker & Andrews 1985; Paola & Seal 1995) is employed here:

$$D = 2^{\Psi}, \qquad \Psi = \log_2 D = \frac{\ln(D)}{\ln(2)}. \tag{4.2a,b}$$

A simple three-layer model is used to treat the bedload transport of heterogeneous sediment. The top layer consists of moving grains participating in the bedload itself. The middle layer is the 'active' or 'exchange' layer, consisting of those immobile grains exposed at the interface between the sediment bed and the flowing fluid, and those smaller unexposed grains that would be exposed to the flow were the larger exposed grains to be moved. The active layer, then, constitutes the reservoir of immobile grains that is readily available for entrainment into the bedload. The bottom layer consists of substrate. This structure is illustrated in figure 4.

The active layer is taken to be sufficiently thin to allow the neglect of vertical structure. The mass grain size density in the active layer at any point (x, z) and time t is here denoted as $F(\Psi, x, z, t)$, where by definition

$$\int_{-\infty}^{\infty} F(\Psi)\mathrm{d}\Psi = 1. \tag{4.3}$$

The first and second moments of this density are of importance in the analysis that follows. The mean grain size Ψ_m and standard deviation σ (on the psi scale) of the active layer are given by

$$\Psi_m = \int_{-\infty}^{\infty} \Psi\, F(\Psi)\mathrm{d}\Psi, \qquad \sigma^2 = \int_{-\infty}^{\infty} (\Psi - \Psi_m)^2 \mathrm{d}\Psi. \tag{4.4a,b}$$

The corresponding geometric mean grain size D_g and geometric standard deviation σ_g are given by

$$D_g = 2^{\Psi_m}, \qquad \sigma_g = 2^{\sigma}. \tag{4.5a,b}$$

In most treatments the thickness of the active layer L_a is taken to be some order-one multiple of D_{90}, i.e. the size such that 90% of the mass of a representative sample is finer. Here a similar formulation is introduced with the use of the moments presented above. The thickness of the active layer L_a is given as

$$L_a = n_a D_\sigma \tag{4.6a}$$

where D_σ is defined as

$$D_\sigma = D_g \sigma_g = 2^{(\Psi_m + \sigma)} \tag{4.6b}$$

and n_a is an order-one constant. In the case of a log-normally distributed sediment D_σ becomes identical to D_{84}, and thus close to D_{90}. A value near unity is commonly assumed for n_a (e.g. Parker 1991*a*).

Roughness height k_s, and thus the distance above the bed for zero velocity R introduced in (3.3) are also taken to be related to D_σ such that

$$k_s = n_k D_\sigma, \qquad R = \frac{n_k}{30} D_\sigma \tag{4.7a,b}$$

where n_k is an order-one constant. Appropriate values for n_k range from 2 to 3.5 (e.g. Bray 1982).

In the case of the present three-layer model the grain size specific Exner equation of sediment mass conservation can be written as

$$(1 - \lambda_p)\left[f_l \frac{\partial B_b}{\partial t} + \frac{\partial (L_a F)}{\partial t}\right] = -\frac{\partial q_x}{\partial x} - \frac{\partial q_z}{\partial z}. \tag{4.8}$$

Here B_b denotes the elevation of the bottom of the active layer, as shown in figure 4; thus

$$B_b + L_a = B. \tag{4.9}$$

In addition $q_x(\Psi, x, z, t)$ and $q_z(\Psi, x, z, t)$ denote the mass bedload transport rate density for size Ψ in the active layer in the x- and z-directions, respectively. These are defined such that the total mass bedload transport rate in the x- and z-directions q_{xT} and q_{zT} are given by the respective forms

$$q_{xT} = \int_{-\infty}^{\infty} q_x \mathrm{d}\Psi, \qquad q_{zT} = \int_{-\infty}^{\infty} q_z \mathrm{d}\Psi. \tag{4.10a,b}$$

The parameter f_l denotes the size density of sediment at the interface between the surface and the substrate that is exchanged as the bed aggrades or degrades. Finally λ_p denotes bed porosity, here taken to be constant.

Variation in the streamwise direction can be neglected in a formulation of the problem of streaks. In light of the fact that the bed is subjected to only slight amounts of aggradation or degradation in the present linear analysis of streak formation, f_l is here simply equated to F. With these simplifications and (4.9) it is seen that (4.8) reduces to

$$(1 - \lambda_p)\left(F \frac{\partial B}{\partial t} + L_a \frac{\partial F}{\partial t}\right) = -\frac{\partial q_z}{\partial z}. \tag{4.11}$$

Further progress requires a relation for transverse bedload transport density q_z. In order to specify this parameter, however, it is first necessary to adopt a form for streamwise sediment transport density q_x. An appropriate equation for the unidirectional bedload transport of heterogeneous sediment is given in Parker (1990*a*), according to which the magnitude and size distribution of the bedload transport is related to the boundary shear stress of the flow and the size distribution of bed material available for transport, i.e. in the active layer. For the purpose of exposition, a flow field that is directed in the streamwise (x) direction and is uniform in the streamwise and transverse (z) directions is considered. The streamwise boundary shear stress, i.e. the value of τ_{xy} evaluated at the bed is here denoted as τ_b.

In the relation of Parker (1990*a*), the bedload transport density of a given size Ψ is taken to be related linearly to the availability of that size in the active layer for

transport. That is,

$$q_x = q_{ux} F, \tag{4.12}$$

where q_{ux} denotes the streamwise transport density per unit content in the active layer. The relation for q_{ux} is

$$q_{ux}^* = 0.00218\,\theta^{3/2}\,G(\zeta), \tag{4.13a}$$

where

$$q_{ux}^* = \frac{q_{ux}}{((s-1)gD_g)^{1/2}\,D_g} \tag{4.13b}$$

denotes a dimensionless Einstein unit bedload transport density and the function $G(\zeta)$ is given as

$$G(\zeta) = \begin{cases} 5474(1-0.853/\zeta)^{4.5}, & \zeta > 1.59 \\ \exp[14.2(\zeta-1) - 9.28(\zeta-1)^2], & 1 \leqslant \zeta \leqslant 1.59 \\ \zeta^{14.2}, & \zeta < 1, \end{cases} \tag{4.13c}$$

where

$$\zeta = \omega \frac{\theta}{\theta_r} \left(\frac{D}{D_g}\right)^{-\beta}. \tag{4.13d}$$

In the above relations,

$$\theta = \frac{\tau_b}{\rho(s-1)gD_g} \tag{4.13e}$$

denotes the Shields stress based on the geometric mean size of the surface layer, s denotes the specific density of the sediment, the dimensionless constants θ_r and β take the values

$$\theta_r = 0.0386, \qquad \beta = 0.0951 \tag{4.13f,g}$$

and

$$\omega = 1 + \frac{\sigma}{\sigma_{oc}}(\omega_{oc} - 1) \tag{4.13h}$$

where σ_{oc} and ω_{oc} are specified functions of θ that can be found in Parker (1990*b*).

In the case of interest here, bedload transport may be directed in the transverse as well as streamwise directions in response to the secondary flow. A transverse bedload transport density per unit content in the active layer q_{uz} can be defined similarly to (4.12);

$$q_z = q_{uz} F. \tag{4.14}$$

A generalized fully nonlinear form for the bedload transport vector (q_{ux}, q_{uz}) is not presently available (but see Kovacs & Parker (1994) for such a relation for uniform sediment). The linearized treatment of Parker & Andrews (1985), however, should be adequate for the purposes of the present analysis. Their result can be stated as

$$q_{uz} = q_{ux}\left(\frac{\tau_t}{\tau_b} - \gamma \frac{\partial B}{\partial z}\right). \tag{4.15}$$

In the above relation τ_t denotes the bed shear stress tangent to the bed and normal to the x-direction, a parameter introduced in the previous section; here it is dimensioned. In addition γ is a parameter governing the tendency of grains to move down transverse slopes under the influence of gravity. The form below was obtained with the use of the formulation of Parker & Andrews (1985), but only after replacing

the hiding function used therein with the one built into the Parker (1990*a*) bedload formulation:

$$\gamma = \widehat{\gamma}\left(\frac{\theta}{\theta_r}\right)^{-1/2}\left(\frac{D}{D_g}\right)^{\beta/2}. \tag{4.16}$$

The constant $\widehat{\gamma}$ in the above relation can be evaluated by imposing concordance with the relation of Johannesson & Parker (1989) for uniform sediment, yielding the result

$$\widehat{\gamma} = 2.67. \tag{4.17}$$

5. Formulation of the linear stability problem

In this section a linearized treatment of sediment transport of heterogeneous mixtures is combined with the linearized flow solution of §3 to determine a dispersion relation governing the stability of longitudinal bed streaks associated with transverse variation in both elevation and roughness.

In accordance with the linearized flow analysis of §3, the bed surface size distribution $F(\Psi, x, z, t)$ is assumed to consist of a spatially uniform distribution $F_0(\Psi)$ plus a perturbed part associated with a streak-like flow perturbation:

$$F = F_0(\Psi)[1 + \epsilon f(\Psi)E(t)C(z)]. \tag{5.1}$$

Insofar as both F and F_0 must satisfy (4.3), it follows that

$$\int_{-\infty}^{\infty} F_0(\Psi)\mathrm{d}\Psi = 1, \qquad \int_{-\infty}^{\infty} F_0(\Psi)f(\Psi)\mathrm{d}\Psi = 0. \tag{5.2a,b}$$

Surface mean size Ψ_m can likewise be decomposed as follows according to (4.4*a*) and (5.1):

$$\Psi_m = \Psi_{m0} + \epsilon\Psi_{m1}E(t)C(z) \tag{5.3a}$$

where

$$\Psi_{m0} = \int_{-\infty}^{\infty} \Psi F_0(\Psi)\mathrm{d}\Psi, \qquad \Psi_{m1} = \int_{-\infty}^{\infty} \Psi F_0(\Psi)f(\Psi)\mathrm{d}\Psi. \tag{5.3b,c}$$

It proves useful here to use the mean grain size on the psi scale of the base state Ψ_{m0} to define a relative psi size ψ such that

$$\psi = \Psi - \Psi_{m0}. \tag{5.4}$$

With this relation, (5.2) and (5.3*b*, *c*) become, respectively,

$$\int_{-\infty}^{\infty} F_0(\psi)\mathrm{d}\psi = 1, \qquad \int_{-\infty}^{\infty} F_0(\psi)f(\psi)\mathrm{d}\psi = 0, \tag{5.5a,b}$$

$$\Psi_{m0} = \int_{-\infty}^{\infty} \psi F_0(\psi)\mathrm{d}\psi, \qquad \Psi_{m1} = \int_{-\infty}^{\infty} \psi F_0(\psi)f(\psi)\mathrm{d}\psi. \tag{5.5c,d}$$

Expansion and linearization of (4.4*b*) in accordance with (5.1) and (5.4) yields the following results for standard deviation:

$$\sigma = \sigma_0 + \epsilon\sigma_1 E(t)C(z) \tag{5.6a}$$

where

$$\sigma_0^2 = \int_{-\infty}^{\infty} \psi^2 F_0(\psi)\mathrm{d}\psi, \qquad \sigma_1 = \frac{1}{2\sigma_0}\int_{-\infty}^{\infty} \psi^2 F_0(\psi)f(\psi)\mathrm{d}\psi. \tag{5.6b,c}$$

The above relations can be used in conjunction with (4.5*a*) and (4.6*b*) to establish the following linearized forms for D_g and D_σ:

$$D_g = D_{g0} + \epsilon D_{g1} E(t) C(z), \qquad D_\sigma = D_{\sigma 0} + \epsilon D_{\sigma 1} E(t) C(z) \tag{5.7a,b}$$

where

$$D_{g1} = D_{g0} \ln(2) \Psi_{m1}, \qquad D_{\sigma_1} = D_{\sigma_0} \ln(2)(\Psi_{m1} + \sigma_1). \tag{5.7c,d}$$

The grain size D_g and its allies above are assumed to have been made dimensionless in accordance with the recipe introduced in §3. The same assumption applies to other variables appearing henceforth. The above relations can be used to obtain perturbed forms for the thickness of the active layer L_a, roughness height k_s and distance above the bed for zero velocity R. Defining

$$L_a = L_{a0} + \epsilon L_{a1} E(t) C(z), \qquad k_s = k_{s0} + \epsilon k_{s1} E(t) C(z) \tag{5.8a,b}$$

it is found from (4.6), (4.7), (5.7) and the definition for the perturbed form of R introduced in §3 that

$$\frac{L_{a1}}{L_{a0}} = \frac{k_{s1}}{k_{s0}} = r = \ln(2)(\Psi_{m1} + \sigma_1). \tag{5.9}$$

The relation for sediment continuity (4.11) takes the following dimensionless form:

$$F \frac{\partial B}{\partial t} + L_a \frac{\partial F}{\partial t} = -\frac{\partial q_z}{\partial z} \tag{5.10}$$

where time t has been non-dimensionalized so as to absorb the bed porosity term $(1 - \lambda_p)$. Linearizing and reducing with the aid of (3.13), (4.12), (4.14), (4.15), (5.1) and (5.9), the following dispersion relation is obtained:

$$\Omega(b + L_{a0} f) = \alpha^2 q_{w0} [t_b b + t_r \ln(2)(\Psi_{m1} + \sigma_1) - \gamma_0(\psi) b] \tag{5.11}$$

where the parameters q_{w0} and γ_0 correspond to the parameters q_{wx} and γ evaluated for the base flow.

A necessary condition for the formation of longitudinal streaks is $\Omega > 0$. The conditions under which this constraint is satisfied are analysed below.

6. Reduction of the dispersion relation

Let $\xi(\psi)$ denote some function of ψ; the parameter $\overline{\xi}$ is defined such that

$$\overline{\xi} = \int_{-\infty}^{\infty} \xi(\psi) F_0(\psi) \mathrm{d}\psi. \tag{6.1}$$

The dispersion relation (5.11) includes the unknowns b, Ψ_{m1}, σ_1, and f as well as the eigenvalue Ω. The parameters Ψ_{m1} and σ_1 are, however, related to f according to (5.5*d*) and (5.6*c*); in addition the constraint (5.5*b*) must hold. These three constraints can be used to reduce the dispersion relation to three equations in the three unknowns b, Ψ_{m1}, and σ_1 (Parker 1991*b*).

The steps are as follows. Equation (5.11) is first multiplied by $F_0(\psi)$ and integrated over all grain sizes ψ; the resulting relation is simplified using (5.5*a*,*b*). Next, (5.11) is multiplied by $\psi F_0(\psi)$, integrated over all grain sizes, and simplified using (5.5*c*,*d*). Finally, (5.11) is multiplied by $\psi^2 F_0(\psi)$, integrated over all grain sizes, and reduced

with (5.6*b*,*c*). The resulting three equations can be expressed in matrix form as follows:

$$\begin{bmatrix} D_1 - \Omega & D_2 & D_2 \\ D_3 & D_4 - L_{a0}\Omega & D_4 \\ D_5 - \sigma_0^2\Omega & D_6 & D_6 - 2\sigma_0 L_{a0}\Omega \end{bmatrix} \begin{bmatrix} b \\ \Psi_{m1} \\ \sigma_1 \end{bmatrix} = \begin{bmatrix} 0 \\ 0 \\ 0 \end{bmatrix} \tag{6.2}$$

where

$$D_1 = \alpha^2 (\overline{q_{u0}} t_b - \overline{q_{u0}\gamma_0}), \qquad D_2 = \alpha^2 \overline{q_{u0}} t_r \ln(2), \tag{6.3a,b}$$

$$D_3 = \alpha^2 (\overline{q_{u0}\psi} t_b - \overline{q_{u0}\gamma_0\psi}), \qquad D_4 = \alpha^2 \overline{q_{u0}\psi} t_r \ln(2), \tag{6.3c,d}$$

$$D_5 = \alpha^2 \left(\overline{q_{u0}\psi^2} t_b - \overline{q_{u0}\gamma_0\psi^2}\right), \qquad D_6 = \alpha^2 \overline{q_{u0}\psi^2} t_r \ln(2), \tag{6.3e,f}$$

and the terms with overbars are defined in accordance with (6.1).

It is of value to first consider the limiting case of uniform sediment, for which

$$F_0(\psi) = \delta(\psi), \qquad f(\psi) = 0 \tag{6.4}$$

and δ denotes the Dirac function. It follows from the above relations that for this case $\Psi_{m1} = \sigma_1 = D_3 = D_4 = D_5 = D_6 = 0$, so that (6.2) reduces to

$$\Omega = D_{10} \tag{6.5a}$$

where

$$D_{10} = \alpha^2 (q_{u0} t_b - q_{u0}\gamma_0)|_{\psi=0} \equiv \alpha^2 q_{u00}(t_b - \gamma_{00}). \tag{6.5b}$$

This limiting case was studied in detail by Colombini (1993).

In the case of heterogeneous sediment, the solvability condition for (6.2) is

$$\det \begin{bmatrix} D_1 - \Omega & D_2 & D_2 \\ D_3 & D_4 - L_{a0}\Omega & D_4 \\ D_5 - \sigma_0^2\Omega & D_6 & D_6 - 2\sigma_0 L_{a0}\Omega \end{bmatrix} = 0. \tag{6.6}$$

Although the resulting characteristic polynomial for Ω would appear to be third degree, it turns out that, since for $\Omega = 0$ the two rightmost columns are the same, $\Omega = 0$ is always a root. The two remaining roots which are not necessarily zero satisfy the following relation:

$$\Omega^2 - \hat{D}_1\Omega - \hat{D}_2 = 0 \tag{6.7}$$

where

$$\hat{D}_1 = D_1 + \frac{1}{2L_{a0}\sigma_0}(D_6 + 2\sigma_0 D_4 - \sigma_0^2 D_2), \tag{6.8a}$$

$$\hat{D}_2 = \frac{1}{2L_{a0}\sigma_0}[D_2 D_5 - D_1 D_6 + 2\sigma_0(D_2 D_3 - D_1 D_4)]. \tag{6.8b}$$

The roots to (6.7) are evidently

$$\Omega_1 = \lambda_+ \hat{D}_1, \qquad \Omega_2 = \lambda_- \hat{D}_1 \tag{6.9a,b}$$

where λ_+ and λ_- are given by

$$\lambda_\pm = \frac{1}{2}\left[1 \pm \left(1 + 4\frac{\hat{D}_2}{\hat{D}_1^2}\right)^{1/2}\right]. \tag{6.9c}$$

It should be evident from the form of the equations that in the limit of vanishing standard deviation of the base size distribution, Ω_1 approaches the limit for uniform sediment and Ω_2 vanishes. An illustration of this for a specific case is given below.

Note that, once the eigenvalues are known, it is possible to evaluate Ψ_{m1} and σ_1 as functions of b. Eliminating σ_1 from the first two rows of (6.2) we obtain, for example

$$\Psi_{m1} = \frac{D_2 D_3 - D_1 D_4 + D_4 \Omega}{D_2 L_{a0} \Omega} b. \tag{6.10}$$

7. Discretization; solution for the two-size case

The numerical implementation of the above solution requires a discretization of ψ space. Here grain size content is assumed to be spread across N contiguous intervals $(\psi_i, \psi_i + \Delta\psi)$, and the content fraction F_{0i} in the ith interval of the base size distribution is defined to be

$$F_{0i} = F_0(\psi_i)\Delta\psi.$$

This corresponds to a density $F_0(\psi)$ that consists of the sum of a forest of weighted Dirac functions

$$F_0(\psi) = \sum_{i=1}^{N} F_{0i}\delta(\psi - \psi_i). \tag{7.1}$$

The definition (6.1) thus takes the discretized form

$$\overline{\xi} = \sum_{i=1}^{N} \xi(\psi_i) F_{0i}. \tag{7.2}$$

The simplest case of heterogeneous sediment of interest is that of a mixture of just two sizes, with only a small difference in size between the two, and with equal content of both in the base size distribution. To this end grain sizes Ψ_1 and Ψ_2 are defined such that

$$\Psi_1 = \Psi_{m0} - \psi^*, \qquad \Psi_2 = \Psi_{m0} + \psi^*, \qquad F_{01} = F_{02} = \tfrac{1}{2} \tag{7.3a,b,c}$$

where ψ^* is taken to be a small parameter. It can be immediately established from (5.3*b*,*c*), (5.4), (5.5), (5.6*b*,*c*) and (7.1) that

$$\psi_1 = -\psi^*, \qquad \psi_2 = \psi^*, \qquad \sigma_0 = \psi^*, \tag{7.3d,e,f}$$

$$f_1 + f_2 = 0, \qquad \Psi_{m1} = -f_1\psi^*, \qquad \sigma_1 = 0. \tag{7.3g,h,i}$$

Since ψ^* is a small parameter, the functions $q_{u0}(\psi)$ and $\gamma_0(\psi)$ need only be evaluated for small values of ψ. Grain size D can thus be expressed as

$$D = \exp[\ln(2)\Psi] = \exp[\ln(2)(\Psi_{m0} + \psi)] \approx D_{g0}[1 + \ln(2)\psi]. \tag{7.4}$$

Expanding the forms for q_{u0} and γ_0 in ψ yields the following results at linear level:

$$q_{u0} = q_{u00}(1 - Q_1\psi), \qquad \gamma_0 = \gamma_{00}(1 + Q_2\psi) \tag{7.5a,b}$$

where

$$q_{u00} = q_{u0}\big|_{D=D_{g0}}, \qquad \gamma_{00} = \gamma_0\big|_{D=D_{g0}} \tag{7.5c,d}$$

and

$$Q_1 = N_0\beta\ln(2), \qquad Q_2 = \tfrac{1}{2}\beta\ln(2) \tag{7.5e,f}$$

where the parameter N_0, defined as

$$N_0 = \frac{\zeta}{G}\frac{\mathrm{d}G}{\mathrm{d}\zeta} \tag{7.5g}$$

is evaluated at the base flow and with $D = D_{g0}$. The form for N_0 is readily obtained from (4.13*c*). Here both parameters Q_1 and Q_2 are positive, with Q_2 taking the constant value of 0.033 and Q_1 varying from 0.936 at very low transport rates to 0 in the limit of infinite transport rate.

Substituting (7.5) into (6.3) and reducing with (6.8) and (6.9), the following approximate results are obtained:

$$\Omega_1 = \alpha^2 q_{u00}\left[(t_b - \gamma_{00}) - \frac{\psi^{*2}}{L_{a0}} t_r \ln(2)\left(\frac{Q_2\gamma_{00}}{t_b - \gamma_{00}} + Q_1\right)\right], \tag{7.6a}$$

$$\Omega_2 = \alpha^2 q_{u00}\frac{\psi^{*2}}{L_{a0}} t_r \ln(2)\frac{Q_2\gamma_{00}}{t_b - \gamma_{00}}. \tag{7.6b}$$

Note that Ω_1 approaches the value for uniform sediment, and Ω_2 approaches 0 as $\psi^* \to 0$.

From (6.10) we can now evaluate Ψ_{m1} as function of b for the two eigenvalues Ω_1 and Ω_2. We obtain

$$\Psi^1_{m1} = -\psi^{*2}\frac{1}{L_{a0}}\left(\frac{Q_2\gamma_{00}}{t_b - \gamma_{00}} + Q_1\right) b, \tag{7.7a}$$

$$\Psi^2_{m1} = -\frac{t_b - \gamma_{00}}{t_r \ln(2)} b. \tag{7.7b}$$

8. Discussion of results

The theory presented in the previous section for the case of 'weak' sorting allows a simple explanation of the mechanism of formation of sand ribbons.

First of all we recall that the theory for homogeneous sediment (Colombini 1993) shows the existence of a critical threshold for the unperturbed Shields stress θ_{0c} above which instability occurs. Marginal conditions are obtained, for the uniform-sediment solution, when

$$\Omega = D_{10} = \alpha^2 q_{u00}(t_b - \gamma_{00}) = 0, \tag{8.1}$$

or equivalently when

$$t_b = \gamma_{00}. \tag{8.2}$$

Using (8.2) it is possible to determine θ_{0c} for every fixed value of the other parameter D_{g0}. Under these conditions, equations (7.6) and (7.7) become singular. Nevertheless, far from marginal conditions for uniform sediment, they clearly show how relaxing the hypothesis of homogeneous sediment modifies the stability plot.

We will analyse two cases, one for which $t_b < \gamma_{00}$ so that the theory for homogeneous sediment does not predict instability, and a second one for which $t_b > \gamma_{00}$, so that the uniform-sediment theory predicts instability for perturbations in a selected range of wavenumbers.

When $t_b - \gamma_{00} < 0$, it follows from (7.6*b*) that Ω_2 is positive, t_r being always negative. If, on the other hand, $t_b - \gamma_{00}$ is positive, (7.6*a*) shows that Ω_1 is positive, and greater than D_{10} so that an increased growth rate with respect to the homogeneous sediment is found.

It can easily be shown that as θ_0 approaches θ_r, q_{u00} falls quite rapidly toward zero,

and thus towards a situation of neutral stability. When the sediment is heterogeneous, then, even for weakly sorted mixtures, instability occurs regardless the value of the unperturbed Shields stress, provided that the grains are allowed to move.

The physical explanation of the increased instability found for the case of heterogeneous sediment is contained in (7.7), which show that, assuming b positive, Ψ^1_{m1} and Ψ^2_{m1} are negative when the correspondent eigenvalue is positive. Recalling the expansions (3.2c) and (5.3a) it can be seen that a negative value of Ψ_{m1} corresponds to a perturbation of the surface size distribution associated with an excess of finer sediment over the crests. In this configuration, which is always observed experimentally, the near-bed secondary flow driven by roughness variations is directed in the same way as the secondary flow driven by variations of bed elevation, leading to an increased amplification.

Two earlier analyses of longitudinal streaks, i.e. Kuroki & Kishi (1981) and Tsujimoto (1989) have relied on one or both of the following *a priori* assumptions in order to close the problem and explain the phenomena: (a) a rhythmic transverse variation in bed elevation generates a secondary flow directed from trough to crest; (b) a rhythmic variation in bed roughness generates a secondary flow from rough to smooth. These assumptions, which are empirically justified, provide plausible starting points for the explanation of streaks in the absence of a flow model appropriate to the problem. In a complete treatment, however, statements (a) and (b) would constitute part of the conclusions rather than assumptions. The present analysis is complete in this regard, in that both the streaks and the observed pattern of secondary flow are predicted from the same model, which is presented in mathematically closed form, and with no unnecessary assumptions.

The behaviour of the eigenvalues just discussed for the case of weak heterogeneity is confirmed for the case of arbitrary σ_0, as shown in figure 5. The two plots have been obtained using the complete solution for two fractions and are thus also valid in the vicinity of marginal conditions for the homogeneous case. Figure 5(a) shows a case for which the unperturbed Shields stress is above the critical threshold for instability in the homogeneous case. The dashed-dotted line represents the case of no heterogeneity, and shows that perturbations of bed elevation only are indeed unstable (positive growth rate) with a maximum growth rate for a value of the wavenumber α close to 4.8 (corresponding to a wavelength of about 1.3 times the unperturbed flow depth). The solid, dashed and dotted lines show the behaviour of the two eigenvalues of the heterogeneous case, for increasing values of the standard deviation σ_0. One of the two eigenvalues is always positive and greater than the homogeneous one, leading to instability for every value of the wavenumber. The wavenumber corresponding to the maximum growth rate is practically unaffected by changes in the standard deviation.

When the bed is composed of heterogeneous sediment, then, the growth rate is increased, owing to the destabilizing effect related to changes in bed roughness that are consequences of the process of sorting. This effect is larger for increased values of the standard deviation of the mixture.

In figure 5(b) an analogous plot is presented for a value of the unperturbed Shields stress below the critical threshold for instability for the homogeneous case. In the case of heterogeneous sediment, instability is again found for every value of the wavenumber. The wavelength of maximum amplification does not seem to be altered much by changes in either the standard deviation or the unperturbed Shields stress.

The prediction of a ratio of wavelength to depth of 1.3 compares with numerous measured values between 1 and 2, with the upper limit being more common. The agreement is thus reasonable, although the predicted value is somewhat small.

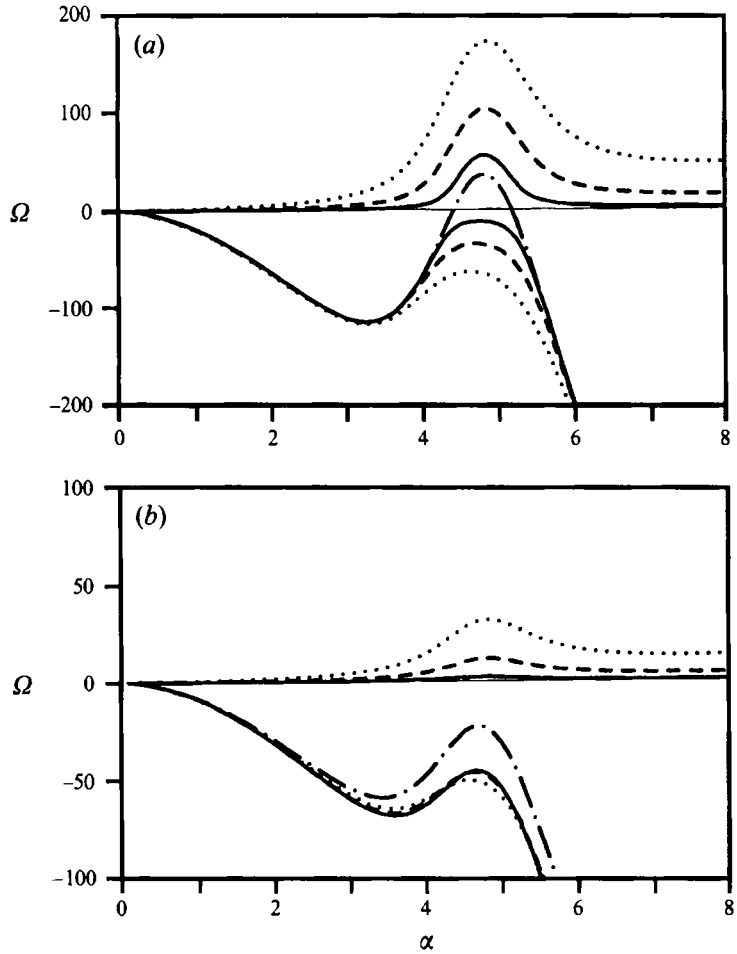

FIGURE 5. Growth rate Ω as function of the wavenumber α for different values of the standard deviation σ_0. (*a*) $\theta_0 > \theta_{0c}$; (*b*) $\theta_0 < \theta_{0c}$. The dashed-dotted line represents the case of homogeneous sediment (or equivalently $\sigma_0 = 0$): ——, $\sigma_0 = 0.2$; – – – –, $\sigma_0 = 0.5$; · · · · · ·, $\sigma_0 = 1$.

The formulation in terms of moments presented in §6 allows the determination of the two eigenvalues of the problem for every assigned distribution of the grain sizes $F_0(\psi)$, the only problem being the evaluation of the integrals (6.3*a–f*) using (6.1). The case of a log-normal distribution of grain-sizes with prescribed standard deviation σ_0 could thus be tackled numerically. When compared to the mixture of two fractions only discussed above, no significant differences in stability characteristics were found for the log-normal case for values of σ_0 up to 3.

Finally, a typical case of a bimodal distribution of sediments was studied and compared with an analogous distribution obtained with two Dirac functions. The densities for the two cases are, respectively,

$$F_0(\Psi) = \frac{F_{01}}{\sigma_{01}(2\pi)^{1/2}} \exp\left[-\frac{(\Psi - \Psi_1)^2}{2\sigma_{01}^2}\right] + \frac{F_{02}}{\sigma_{02}(2\pi)^{1/2}} \exp\left[-\frac{(\Psi - \Psi_2)^2}{2\sigma_{02}^2}\right], \tag{8.3a}$$

$$F_0(\Psi) = F_{01}\delta(\Psi - \Psi_1) + F_{02}\delta(\Psi - \Psi_2) \tag{8.3b}$$

where $F_{01} = 0.3, F_{02} = 0.7, \sigma_{01} = \sigma_{02} = 1, \Psi_1 = -1, \Psi_2 = 2$.

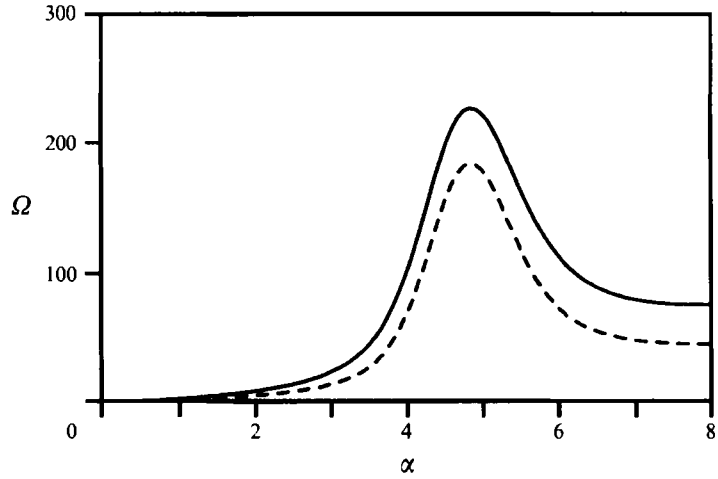

FIGURE 6. Growth rate Ω for the unstable eigenvalue as function of the wavenumber α for a bimodal distribution: ——, continuous distribution; – – –, discrete distribution.

As shown in figure 6 for the unstable eigenvalue, a continuous distribution of sediment leads, in this case, to higher values of the growth rate than those associated with the analogous discrete distribution. The wavenumber for maximum growth rate is again close to 5.

9. Conclusion

The model presented here allows for the formation of stripes that include varying degrees of elevation and roughness variation. It is thus capable of explaining the formation of both elevation and roughness stripes. As opposed to the results of Colombini (1993) for elevation stripes in uniform sediment, the present theory predicts that even a slight degree of sediment heterogeneity results in an instability leading to stripe formation at any Shields stress in excess of the threshold value for sediment motion. A general explanation of the formation of longitudinal streaks over an erodible bed has thus been achieved.

We thank Professor A. Müller who kindly provided the reference to the work of Günter and the photos of figure 1. This research was funded by the Italian Ministero dell'Università e della Ricerca Scientifica e Tecnologica under grants MURST 40% and 60% and by the US National Science Foundation (grant no. CTS-9207882).

REFERENCES

ASHIDA, K. & NARAI, S. 1969 The structure of movable bed configuration. *Bull. Disas. Prev. Res. Inst., Kyoto University* **19**, 15–29.

BRAY, D. I. 1982 Flow resistance in gravel-bed rivers. In *Gravel-Bed Rivers*, pp. 109–133. John Wiley & Sons.

BRADSHAW, P. 1987 Turbulent secondary flows. *Ann. Rev. Fluid Mech.* **19**, 53–74.

COLOMBINI, M. 1993 Turbulence-driven secondary flows and formation of sand ridges. *J. Fluid Mech.* **254**, 701–719.

DEMUREN, A. O. & RODI, W. 1984 Calculation of turbulence-driven secondary motion in non-circular ducts. *J. Fluid Mech.* **140**, 189–222.

DE VRIEND, H. J. 1977 A mathematical model of steady flow in curved shallow channels. *J. Hydraul. Res.* **15**, 37–54.

GATSKI, T. B. & SPEZIALE, C. G. 1993 On explicit algebraic stress models for complex turbulent flows. *J. Fluid Mech.* **254**, 59–78.

GÜNTER, A. 1971 Die kritische mittlere Sohlenschubspannung bei Geschiebemischungen unter Berücksichtigung der Deckschichtbildung und der turbulenzbedingten Sohlenschubspannungsschwankungen'. *Mitteilung der Versuchsanstalt für Wasserbau an der ETH Zurich*, vol. 3.

HINZE, J. O. 1973 Experimental investigation of secondary currents in the turbulent flow through a straight conduit. *Appl. Sci. Res.* **28**, 453–465.

IKEDA, S. 1981 Self-formed straight channels in sandy beds. *J. Hydraul. Div. ASCE* **107**, 389–406.

JOHANNESSON, H. & PARKER, G. 1989 Linear theory of river meanders. In *River Meandering*. AGU Water Resources Monograph, vol. 12, pp. 181–213.

KINOSHITA, R. 1967 An analysis of the movement of flood waters by aerial photography, concerning characteristics of turbulence and surface flow. *Photographic Surveying* **6**, 1–17.

KOVACS, A. & PARKER, G. 1994 A new vectorial bedload formulation and its application to the time evolution of straight rivers. *J. Fluid Mech.* **267**, 153–183.

KUROKI, M. & KISHI, T. 1981 Structures of longitudinal vortices in wide open channels. *Trans. JSCE* **13**, 176–179.

MCLEAN, S. R. 1981 The role of non-uniform roughness in the formation of sand ribbons. *Mar. Geol.* **42**, 49–74.

MÜLLER, A. & STUDERUS, X. 1979 Secondary flow in an open channel. *Proc. 18th IAHR Congress, Cagliari, Italy*, pp. B19–B24.

NAOT, D. & RODI, W. 1982 Calculation of secondary currents in channel flow. *J. Hydraul. Div. ASCE* **108**, 948–968.

NEZU, I. & NAKAGAWA, H. 1984 Cellular secondary currents in straight conduit. *J. Hydraul. Engng ASCE* **110**, 173–193.

PAOLA, C. & SEAL, R. 1995 Grain-size patchiness as a cause of selective deposition and downstream fining. *Water Resources Res.* **31**, 1395–1407.

PARKER, G. 1990*a* Surface-based bedload transport relation for gravel rivers. *J. Hydraulic Res.* **28**, 417–436.

PARKER, G. 1990*b* The "ACRONYM" series of Pascal programs for computing bedload transport in gravel rivers. External Memo. M-220. St. Anthony Falls Hydraulic Laboratory, University of Minnesota.

PARKER, G. 1991*a* Selective sorting and abrasion of river gravel. I: Theory. *J. Hydraul. Engng ASCE* **117**, 131–149.

PARKER, G. 1991*b* Some random notes on grain sorting. *Proc. Grain Sorting Seminar, IAHR, Ascona Switzerland*, pp. 20–76.

PARKER, G. & ANDREWS, E. D. 1985 Sorting of bed load sediment by flow in meander bends. *Water Resources Res.* **21**, 1361–1373.

PARKER, G. & SUTHERLAND, A. 1990 Fluvial armor. *J. Hydraul. Res.* **28**, 529–544.

SPEZIALE, C. G. 1987 On nonlinear K–l and K–ϵ models of turbulence. *J. Fluid Mech.* **178**, 459–475.

TOMINAGA, A. & NEZU, I. 1991 The effects of secondary currents on sediment transport in open-channel flows. *Proc. Intl Symp. on The Transport of Suspended Sediment and its Mathematical Modelling, Florence, Italy*, pp. 253–264.

TSUJIMOTO, T. 1989 Longitudinal stripes of sorting due to cellular secondary currents. *J. Hydrosci. Hydraul. Engng* **7**, 23–34.

WOLMAN, M. G. & BRUSH, L. M. 1961 Factors controlling the size and shape of stream channels in coarse noncohesive sands. *Geological Survey*, US Geological Survey, Prof. Paper 282–G.